

UNVEILING OBSCURED ACCRETION IN THE CHANDRA DEEP FIELD SOUTH

F. FIORE¹, A. GRAZIAN¹, P. SANTINI^{1,2}, S. PUCCHETTI^{3,1}, M. BRUSA⁴, C. FERUGLIO¹, A. FONTANA¹, E. GIALLONGO¹, A. COMASTRI⁵, C. GRUPPIONI⁵, F. POZZI⁵, G. ZAMORANI⁵, C. VIGNALI⁶

Draft version April 23, 2007

ABSTRACT

A large population of heavily obscured, Compton Thick AGNs is predicted by models of galaxy formation, models of Cosmic X-ray Background and by the “relic” super-massive black-hole mass function measured from local bulges. However, so far only a handful of Compton thick AGNs have been possibly detected using even the deepest Chandra and XMM surveys. Compton-thick AGNs can be recovered thanks to the reprocessing of the AGN UV emission in the infrared by selecting sources with AGN luminosity’s in the mid-infrared and faint near-infrared and optical emission. To this purpose, we make use of deep HST, VLT, Spitzer and Chandra data on the Chandra Deep Field South to constrain the number of Compton thick AGN in this field. We show that sources with high $24\mu\text{m}$ to optical flux ratios and red colors form a distinct source population, and that their infrared luminosity is dominated by AGN emission. Analysis of the X-ray properties of these extreme sources shows that most of them are indeed likely to be highly obscured, Compton thick AGNs. The number of infrared selected, Compton thick AGNs with infrared luminosity higher than $10^{44.8} \text{ erg s}^{-1}$ turns out to be roughly similar to that of X-ray selected, unobscured and moderately obscured AGNs in the redshift bin 1.2-2.6. This “factor of 2” source population is exactly what it is needed to solve the discrepancies between model predictions and X-ray AGN selection.

Subject headings: Active Galactic Nuclei

1. INTRODUCTION

Active Galactic Nuclei (AGN) are not only witnesses of the phases of galaxy formation and/or assembly, but are most likely among leading actors. Indeed, three seminal discoveries indicate tight links and feedbacks between super-massive black holes (SMBH), nuclear activity and galaxy evolution. The first is the discovery of SMBH in the center of most nearby bulge dominated galaxies, and the tight correlation between their masses and galaxy bulge properties (Gebhardt et al. 2000, Ferrarese & Merritt 2000, Marconi & Hunt 2003 and references therein). The second is that the growth of SMBH is mostly due to accretion of matter during their active phases, and therefore that most bulge galaxies passed a phase of strong nuclear activity (Soltan 1982, Marconi et al. 2004). The third is that the evolution of AGN is luminosity dependent, with lower luminosity AGN peaking at a redshift lower than luminous QSOs (Hasinger 2003, 2005, Fiore et al. 2003, Ueda et al. 2003, La Franca et al. 2005, Brandt & Hasinger 2005, Bongiorno et al. 2007), a bimodal behavior recalling the evolution of star-forming galaxies and that of massive spheroids (Cowie et al. 1996, Franceschini et al. 1999, De Lucia et al. 2006). All three discoveries imply that obtaining a complete census of accreting SMBH through the cosmic epochs and constraining accretion efficiency and feedbacks are crucial steps toward the understanding of Galaxy formation

and evolution.

First attempts to constrain models for the formation and evolution of structure in the Universe using the evolving optical and X-ray AGN luminosity functions have been presented by Granato et al. (2001, 2004), Di Matteo et al. (2005), and Menci et al. (2004, 2005). In particular, the latter model links the evolution of the galaxies in the hierarchical clustering scenarios with the changing accretion rates of cold gas onto the central SMBH that power the QSO (Cavaliere & Vittorini 2000). The results of this model were encouraging, in the sense that it predicts a trend of lower luminosity AGN to peak at increasingly lower redshift, as observed. However, from a quantitative point of view, the model overpredicts by a factor of about 2 the space density of low-to-intermediate luminosity (Seyfert like) AGNs at $z=1.5-2.5$ with respect to present X-ray observations. Furthermore, Marconi et. al. (2004, 2007 in preparation) derived a SMBH mass function from the X-ray selected AGN luminosity functions (e.g. La Franca et al. 2005) that falls short by a factor of about 2 to the “relic” SMBH mass function, evaluated using the $M_{BH} - \sigma_V / M_{BH} - M_B$ relationships and the local bulge’s luminosity function. The most likely explanation for both discrepancies is that present X-ray surveys, although very efficient to probe unobscured and moderately obscured AGN (with column densities up to a few 10^{23} cm^{-2} , the so-called Compton thin AGNs), miss most of the very highly obscured, but still strongly accreting objects, the so called Compton Thick AGNs, with a column density $N_H \gtrsim 10^{24} \text{ cm}^{-2}$ (see Comastri 2004). Indeed, only a handful of the faintest sources in the Chandra deep fields may be Compton thick (see La Franca et al. 2005 and Tozzi et al. 2006). So we still may be viewing just the tip of the iceberg of the highly obscured AGN population. Compton thick objects may well be more common at high redshift, as

Electronic address: fiore@oa-roma.inaf.it

¹ INAF-OAR, via Frascati 33, Monteporzio, I00040, Italy

² Universita’ di Roma La Sapienza, Italy

³ ASI Science data Center, ASDC c/o ESRIN, via G. Galilei, 00044 Frascati, Italy

⁴ Max Planck Institut für extraterrestrische Physik, Giessenbachstrasse 1, D-85748 Garching bei München, Germany

⁵ INAF-OABO, via Ranzani 1, Bologna, Italy

⁶ Universita’ di Bologna, via Ranzani 1, Bologna, Italy

suggested on theoretical ground by Silk & Rees (1998) and Fabian (1999) and on observational ground by e.g. Gilli et al. (2001), Worsley et al. (2004, 2006), and La Franca et al. (2005).

Compton thick AGN at $z \gtrsim 1$ can be recovered thanks to the reprocessing of the AGN UV emission in the infrared by selecting sources with AGN luminosities in the mid-infrared and faint near-infrared and optical emission (e.g. Martinez-Sansigre et al. 2005, 2006, Houck et al. 2005, Weedman et al. 2006a, 2006b). We investigate further this issue making use of the multiwavelength data obtained on the Chandra Deep Field South (Giacconi et al. 2002), one of the fields with the deepest coverage at optical, infrared and X-ray wavelengths. Preliminary results of this work have been presented at the November 2006 Chandra workshop on Extragalactic Surveys⁷. A $H_0 = 70 \text{ km s}^{-1} \text{ Mpc}^{-1}$, $\Omega_M = 0.3$, $\Omega_\Lambda = 0.7$ cosmology is adopted throughout.

2. DATASETS AND SAMPLE SELECTION

The selection and spectroscopic identification of complete AGN samples from mid-IR surveys is a rather difficult task, because AGNs make only a small fraction of the full mid-IR source population. Using Spitzer IRAC colors results in samples significantly contaminated by star-forming galaxies (e.g. Lacy et al. 2004, Alonso-Herrero et al. 2006, Barmby et al. 2006, Polletta et al. 2006). Comparing the global observed Spectral Energy Distribution (SED) to AGN and galaxy templates proved to be more efficient in selecting AGN samples (Polletta et al. 2006, 2007). However, it is very difficult to assess the completeness of these samples given all complex selection effects. Furthermore, many obscured AGN may still be anyway missed by this technique. Here we adopt a different approach. We do not pretend to select *all* AGN through optical and infrared photometry. As explained before X-rays are much more efficient in selecting unobscured and moderately obscured AGN. We concentrate our effort on highly obscured AGN only and we limit our analysis to the high infrared luminosity AGN population. The driving consideration is that differences between nuclear and star-formation emission are emphasized comparing the observed SEDs with galaxy templates over a range as broad as possible, an approach similar, in this respect, to that of Martinez-Sansigre et al. (2005,2006), Houck et al. (2005) and Weedman et al. (2006). However, we will also make use of deep X-ray data to validate our findings and make them on quantitative grounds.

We use in this paper the latest version of the GOODS-MUSIC catalog (Grazian et al. 2006). With respect to the published version, the revised version of this catalog includes objects that are selected in the $4.5\mu\text{m}$ band only, and the observed flux at $24\mu\text{m}$ for all objects in the catalog, obtained following the procedures described in De Santis et al. (2007). We limit the analysis to the region fully covered by deep VLT/ISAAC near infrared photometry (143.2 arcmin^2) and to the sources with MIPS $24\mu\text{m}$ fluxes $F(24\mu\text{m}) > 40\mu\text{Jy}$ (about 1700 sources). 46 of the sources are selected in the $4.5\mu\text{m}$ IRAC band only, i.e. their z and K magnitudes are below the chosen detection threshold. Only 4 of these sources do not have counterparts in the optical and/or in the near infrared

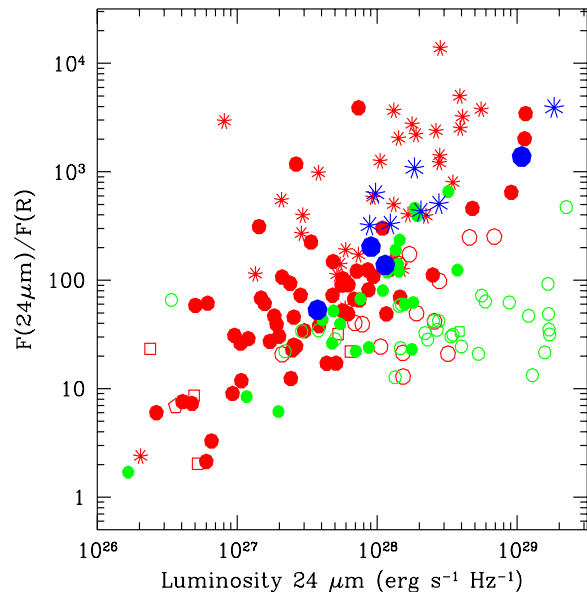


FIG. 1.— MIR/O as a function of the $24\mu\text{m}$ luminosity for three X-ray source samples (GOODS-MUSIC, red points, ELAIS-S1, green points and HELLAS2XMM, large blue points, Pozzi et al. 2007). Open circles = type 1 AGN; filled circles = non type 1 AGN; stars = photometric redshifts. Note that MIR/O of non broad line AGN is strongly correlated with the luminosity at $24\mu\text{m}$.

images. At the flux limits adopted here, we do not detect any objects at $24\mu\text{m}$ that is not detected at shorter wavelengths.

The GOODS-MUSIC catalog includes total infrared luminosities, for the sources with a reliable spectroscopic or photometric redshift, computed by integrating the best fit galaxy and AGN templates between 8 and $1000\mu\text{m}$ and by using the Sanders & Mirabel (1996) relation between $L_{8-1000\mu\text{m}}$ and the four IRAS bands fluxes. These fluxes were estimated by convolving with the IRAS filters the galaxy and AGN templates best fitting the observed 1- $24\mu\text{m}$ SEDs. The two luminosity estimates are consistent one with the other. We used several libraries of galaxy templates to fit the observed SEDs, including passive galaxies, star-forming galaxies, unobscured AGNs and highly obscured AGNs. A particular care was put of course on the latter issue. In addition to the SEDs presented by Polletta et al. (2007) we used the SEDs of the highly obscured AGNs in Pozzi et al. (2007). The total infrared luminosity is dominated by the contributions at wavelengths of $\sim 100 - 1000\mu\text{m}$, well outside the observed band, and where the galaxy and AGN templates can differ one from the other by large factors. Different templates can produce similar fits below $24\mu\text{m}$ but give rise to large differences in the total infrared luminosity. As an example, the total infrared luminosity obtained from the template SED of an extreme star-burst galaxy may be 10-30 times higher than that obtained from AGN SEDs normalized to the same flux at $24\mu\text{m}$. This means that a large systematic uncertainty is associated to each infrared luminosity. However, the average and median luminosities of sufficiently large source samples can be considered as indicative of the population properties of these samples.

⁷ http://cxc.harvard.edu/xsurveys06/agenda/presentations/fabrizio_fiorini

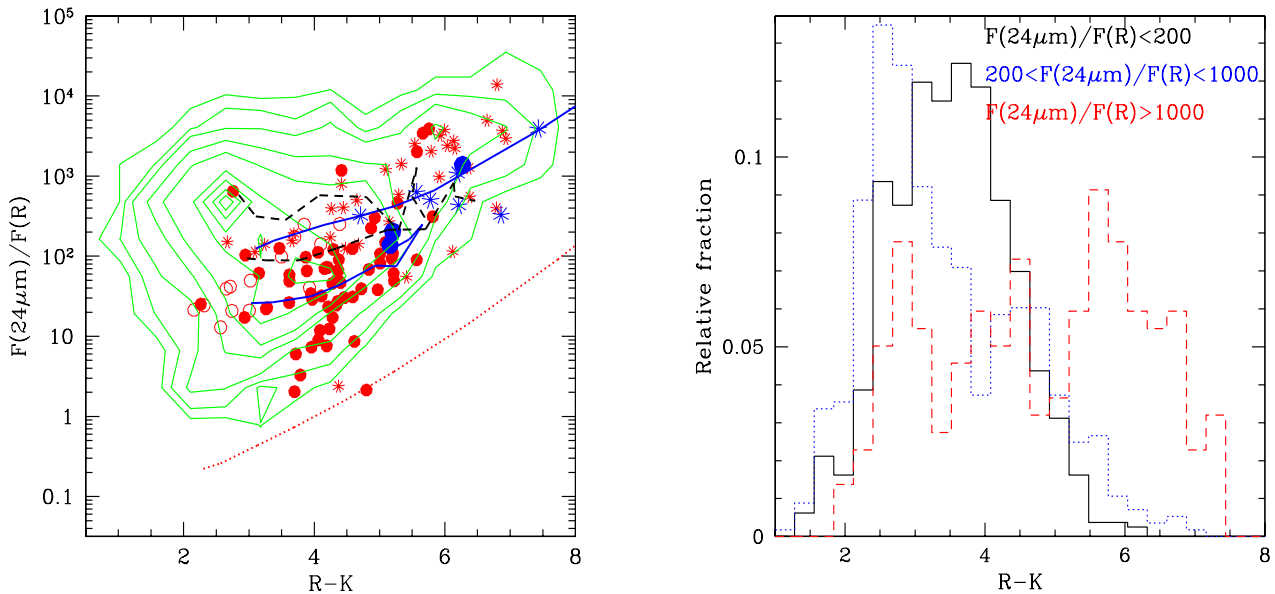


FIG. 2.— Left panel: the MIR/O as a function of the R-K color for two X-ray source samples (GOODS-MUSIC and HELLAS2XMM, large symbols, from Pozzi et al. 2007). Open circles = type 1 AGN; filled circles = non type 1 AGN; stars = photometric redshifts. Isodensity contours of all GOODS-MUSIC $24\mu\text{m}$ sources are overlaid to the plot. The thick continuous lines mark the expectations of two obscured AGN SEDs with redshift increasing from 0 to 4 from left to right. The lower curve represents a typical low luminosity Seyfert 2 galaxy, while the upper curve represents a highly obscured AGN from the Pozzi et al sample (A2690.75). The black dashed lines are the expectations of the SEDs of two star-burst galaxies (M82, lower curve and Arp220, upper curve) for $z=0-4$. The dotted line is the expectation of a passive elliptical galaxy for $z=0-4$. Right panel: fraction of GOODS-MUSIC $24\mu\text{m}$ sources as a function of the R-K color in three MIR/O bins: solid histogram = MIR/O < 200; dotted histogram = $200 < \text{MIR/O} < 1000$; dashed histogram = MIR/O > 1000.

available on the Chandra Deep Fields are the $24\mu\text{m}$ mid-infrared band covered by Spitzer MIPS and the optical band covered by HST ACS. Bright $24\mu\text{m}$ sources with faint optical counterparts must be either luminous AGN whose optical nuclear emission is completely blocked by dust and gas, or powerful dusty-starburst galaxies. The Mid-infrared to optical flux ratio (MIR/O⁸) can therefore be considered a rough estimator of obscured activity in galaxies. Figure 1 shows MIR/O as a function of the $24\mu\text{m}$ luminosity, $L(24\mu\text{m})$, for three samples of X-ray sources. Unobscured AGNs (open symbols in figure 1) have MIR/O in the range 10-200, uncorrelated with $L(24\mu\text{m})$, as expected because the nuclear emission dominates both optical and mid infrared wavelengths. Conversely, obscured AGNs (filled symbols) have MIR/O spanning a broader range, and fairly correlated with $L(24\mu\text{m})$. This behavior resembles that of moderately obscured AGNs detected in X-rays, for which the X-ray to optical flux ratio (X/O) is strongly correlated with the X-ray luminosity (Fiore et al. 2003, Eckart et al. 2006). High X/O ratios were found to be good indicators for X-ray obscuration in high luminosity sources (Fiore et al. 2003, Cocchia et al. 2007). However, Compton thick AGN are faint in X-rays, and cannot be selected using their X/O flux ratio. Interestingly, the MIR/O of X-ray selected sources is strongly correlated with X/O, and therefore it is reasonable to suspect that Compton thick, high luminosity AGN have high MIR/O ratios. Furthermore, since X-ray obscured AGNs tend to have red R-K colors (Brusa et al. 2005 and reference therein),

⁸ $\text{MIR/O} = (F(24\mu\text{m})/F(R))$; $\log F(R) = -0.4 \times R - 22.5467$. R magnitudes have been obtained by interpolating the V and I magnitudes in the GOODS-MUSIC catalog provided by HST/ACS

one would also expect that Compton thick AGN have similarly red colors.

Indeed figure 2 shows that the MIR/O of X-ray selected, obscured AGN is correlated with the R-K color, as expected. Figure 2 also shows the iso-density contours of the GOODS-MUSIC $24\mu\text{m}$ sources with $F(24\mu\text{m}) > 40\mu\text{Jy}$. Intriguingly, the iso-density contours close in toward higher R-K values, and extend toward the region occupied by obscured X-ray selected AGN at high MIR/O and high R-K values. The bimodality at high values of MIR/O of the color distribution of the $24\mu\text{m}$ selected sources is evident in the rightmost panel of figure 2, which shows the fraction of GOODS-MUSIC $24\mu\text{m}$ sources as a function of the R-K color in three MIR/O bins. While at low MIR/O values the distributions are peaked at $R-K \sim 2.5 - 3.5$ and decrease smoothly toward higher R-K values, the distribution of the sources with MIR/O > 1000 shows a strong excess at $R-K > 4.5$. It is interesting to note that most of the highly obscured AGN selected in the HELLAS2XMM survey on the basis of their high X-ray to optical flux ratio (Pozzi et al. 2007) have MIR/O higher than a few hundred, and all have $R-K > 4.5$. Their SEDs are characterized by a passive early-type galaxy in the optical and in the near infrared, and by an AGN component in the mid infrared. These SEDs redshifted up to $z=4$ are able to explain the extreme colors of the MIR/O > 1000 $R-K > 4.5$ sources, unlike the SED of even extreme star-forming galaxies like Arp220 (see figure 2 left panel). This strongly suggests that most of the MIR/O > 1000 $R-K > 4.5$ sources are powered by an active nucleus. Similar conclusions are found analyzing slightly different color diagrams, like MIR/O vs. $F(24\mu\text{m})/F(8\mu\text{m})$ and MIR/O vs. $F(3.6\mu\text{m})/F(Z)$.

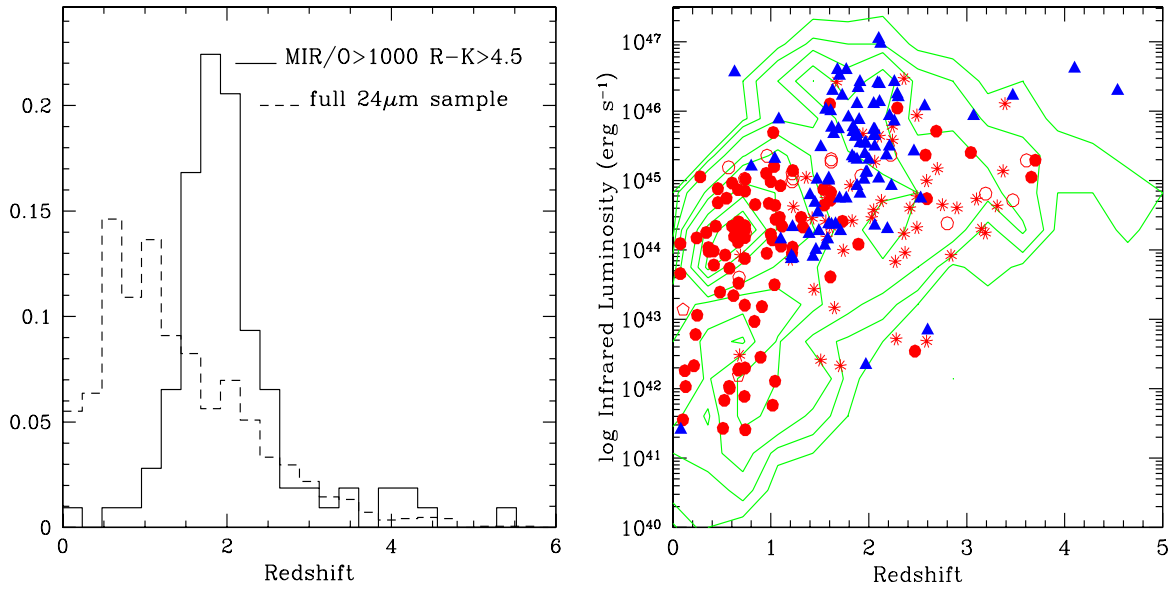


FIG. 3.— Left panel: the redshift distribution of the $\text{MIR}/\text{O} > 1000$ and $\text{R}-\text{K} > 4.5$ sources compared to that of the full GOODS-MUSIC $24\mu\text{m}$ sample. Right panel: the redshift-infrared luminosity plane for the full $24\mu\text{m}$ GOODS-MUSIC source sample (isodensity contours); the CDfS X-ray sample (Open circles = type 1 AGN; filled circles = non type 1 AGN; stars = photometric redshifts); and the sample of $\text{MIR}/\text{O} > 1000$ and $\text{R}-\text{K} > 4.5$ sources with no direct X-ray detection (filled triangles)

3. X-RAY PROPERTIES OF EXTREME $24\mu\text{m}$ SELECTED SOURCES

We selected from the $24\mu\text{m}$ GOODS-MUSIC sample sources with $\text{MIR}/\text{O} > 1000$ and $\text{R}-\text{K} > 4.5$, our candidate extremely obscured AGNs. There are in total 135 such sources. Of these, 18 have an X-ray detection in Alexander et al. (2003). Four other sources are not formally detected but have more than 4-5 counts (after background subtraction) at the position of the $24\mu\text{m}$ source. Three of these 22 sources have a spectroscopic redshift, with a narrow line dominated optical spectrum, the other 19 have a robust photometric redshift in the GOODS-MUSIC catalog ($\Delta z/(1+z) < 0.05$, Grazian et al. 2006); the median redshift (and its interquartile range) are 2.1 (0.5). The median infrared luminosity is $\langle \log L(\text{IR}) \rangle = 45.14$ (0.66). The X-ray luminosities are in all cases higher than 10^{42} erg s^{-1} , making them bona-fide AGNs. The hardness ratios indicate in most cases a hard, possibly obscured X-ray spectrum, and actually they are among the most obscured sources in the Tozzi et al (2006) analysis (all have column densities higher than a few $\times 10^{22}$ cm^{-2} and 2 have columns as high as 10^{24} cm^{-2}). The median logarithmic ratio between the total infrared and the 2-10 X-ray luminosity is 1.77 (0.41). As a comparison, the median logarithmic ratio of the infrared to 2-10 keV luminosity for the full X-ray sample is 1.47 (0.59). The probability that the two distributions are drawn from the same parent population is $\sim 1\%$, using the Kolmogorov-Smirnov test.

The total number of sources with $\text{MIR}/\text{O} > 1000$ and $\text{R}-\text{K} > 4.5$ and no direct X-ray detection considered is 111 (we also excluded 2 sources which happen to lie within 5 arcsec from an X-ray source). Four of these sources have a spectroscopic redshift, 99 have photometric redshift in the GOODS-MUSIC catalog. For four sources we could compute a lower limit to the redshift. For four sources we do not have reliable redshifts or limits. In 67% of the

cases the 1- $24\mu\text{m}$ SED is best fitted by an AGN template (in no case the SEDs is best fitted by a type 1 QSO template). Both median redshift and infrared luminosity are similar to those of the 22 sources with high MIR/O , high $\text{R}-\text{K}$ and an X-ray detection. The redshift and infrared luminosities distributions of the $\text{MIR}/\text{O} > 1000$ and $\text{R}-\text{K} > 4.5$ sources are compared in figure 3 to those of the full GOODS-MUSIC $24\mu\text{m}$ and X-ray selected samples. The $\text{MIR}/\text{O} > 1000$ and $\text{R}-\text{K} > 4.5$ sources have a redshift distribution with median redshift = 1.91 and interquartile 0.30 (excluding the lower limits $\langle z \rangle = 1.90$, 0.28). This distribution is shifted toward higher values than the full GOODS-MUSIC $24\mu\text{m}$ source sample (figure 3 left panel). The right panel of figure 3 shows that moderately obscured X-ray selected sources are concentrated below $z=1.5$ and span a range of infrared luminosities from $\log(\text{IR}) \sim 41.5$ to $\log(\text{LIR}) \sim 45$. Their median 2-10 keV and infrared luminosities are 43.16 (0.56) and 44.71 (0.48) respectively. On the other hand, the $\text{MIR}/\text{O} > 1000$ and $\text{R}-\text{K} > 4.5$ sources are concentrated between $z=1.2$ and $z=2.6$ and have infrared luminosities from $\log(\text{LIR}) \sim 44$ to $\log(\text{LIR}) \sim 47$, systematically higher than X-ray selected sources. Their median infrared luminosity is 45.48 (0.59). Compared to the full GOODS-MUSIC $24\mu\text{m}$ sample, the $\text{MIR}/\text{O} > 1000$ and $\text{R}-\text{K} > 4.5$ sources are concentrated toward the higher infrared luminosities at each redshift. We stress again that large systematic errors are associated to each infrared luminosity, which therefore should not be considered singularly.

3.1. X-ray stacking analysis

Thanks to the low Chandra background, it is possible to increase the effective exposure time and derive average properties of undetected objects, using "stacking" techniques: counts at the positions of known sources are co-added in order to probe X-ray emission substantially

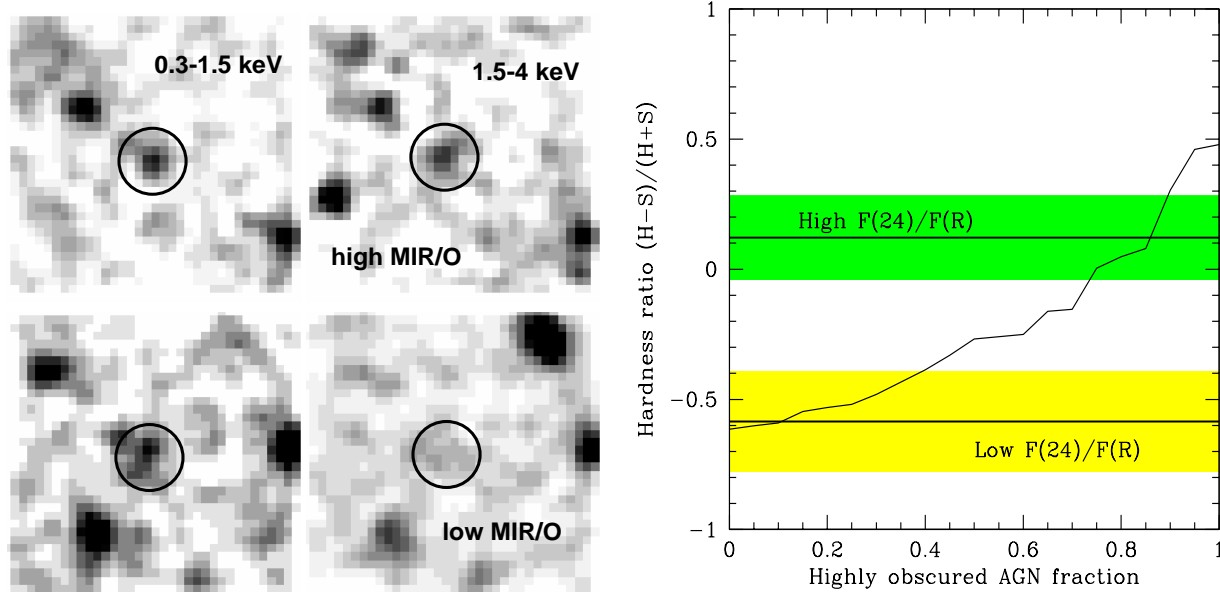


FIG. 4.— Left figure: stacked X-ray images of $24\mu\text{m}$ GOODS-MUSIC sources. Images are have sides of 18 arcsec, central circles have 2 arcsec radii. Upper panels refer to 111 sources with $\text{MIR}/\text{O} > 1000$ and $\text{R-K} > 4.5$; lower panels refer to 73 sources with $\text{MIR}/\text{O} < 200$ and $\text{R-K} > 4.5$. Left panels are stacks in the S 0.3-1.5 keV band, right panels are stacks in the H 1.5-4 keV band. Right figure: the hardness ratio $(\text{H-S})/(\text{H+S})$ of the counts in circles of 2 arcsec radii as a function of the fraction of highly obscured AGN in the sample of 129 $24\mu\text{m}$ GOODS-MUSIC sources with $\text{MIR}/\text{O} > 1000$ and $\text{R-K} > 4.5$. The solid curve is the result of Montecarlo simulations (see text for details); the two thick horizontal lines are the average hardness ratios measured for the $\text{MIR}/\text{O} > 1000$ and $\text{R-K} > 4.5$ (upper line) and $\text{MIR}/\text{O} < 200$ and $\text{R-K} > 4.5$ sources (lower line). The colored bands mark the hardness ratio statistical uncertainties.

below the single source sensitivity limit. To investigate further the X-ray properties of the $\text{MIR}/\text{O} > 1000$ and $\text{R-K} > 4.5$ source sample we performed a stacking analysis of the 111 sources not directly detected in the Chandra 1 Msec X-ray image. As control samples we selected sources with $\text{MIR}/\text{O} > 1000$ and $\text{R-K} < 3.5$ (73 sources after the exclusion of the sources directly detected in the X-ray image) and sources with $\text{MIR}/\text{O} < 200$ and $\text{R-K} > 4.5$ (51 sources).

The top panels of figure 4a) show the X-ray stack of the 111 $24\mu\text{m}$ sources with $\text{MIR}/\text{O} > 1000$ and $\text{R-K} > 4.5$ in two energy bands. This is compared to the stack of 73 sources with $\text{MIR}/\text{O} < 200$ and $\text{R-K} > 4.5$ and no direct X-ray detections (lower panels). We choose the bands 0.3-1.5 keV (soft band, S) and 1.5-4 keV (hard band, H) to keep the level of the internal background as low as possible and similar in the two bands. The stack of the high MIR/O and high R-K sources produces a detection in both soft and hard bands, with count rates $(0.98 \pm 0.20) \times 10^{-6}$ counts/s and $(1.25 \pm 0.26) \times 10^{-6}$ counts/s in the two bands respectively (using a 2 arcsec radius extraction region). The total exposure time for this source sample is 94 Msec. Conversely, the stack of the low MIR/O and high R-K sources produces a significant detection only in the soft band, with count rate $(1.89 \pm 0.32) \times 10^{-6}$ counts/s. The count rate measured in the hard band is $(4.9 \pm 1.9) \times 10^{-7}$ counts/s. No detection in either bands is obtained for the stack of 51 sources with high MIR/O and low R-K , with 1σ upper limits of $\sim 2 \times 10^{-7}$ counts/s. The total exposure times for control samples are 61 Msec and 43 Msec respectively.

We used the observed flux in the stacked images, together with the hardness ratio $\text{H-S}/\text{H+S}$, to constrain the fraction of highly obscured AGN in the samples.

To this purpose, we generated simulated X-ray count rates and hardness ratios as a function of the fraction of the AGN, assuming that the $\text{MIR}/\text{O} > 1000$ and $\text{R-K} > 4.5$ source sample is made by obscured AGNs and star-forming galaxies. We started from the observed redshift and infrared luminosities, and assumed typical values for the infrared to X-ray (2-10 keV) unobscured luminosity ratios. For the AGNs we conservatively used a logarithmic factor of 1.8, equal to the factor found for the $\text{MIR}/\text{O} > 1000$ and $\text{R-K} > 4.5$ sources with an X-ray detection. For star-forming galaxies we used a factor 3.6 (Ranalli et al. 2003). We assumed that the star-forming galaxies are not obscured in X-rays, while the AGNs are highly obscured. We adopted a flat $\log N_H$ distribution from 23 to 26 cm^{-2} . For a given fraction of AGN in the sample, we first decide, using a random generator, whether each source is an AGN or a star-forming galaxy. Then, if the source turned out to be an AGN, we choose an absorbing column density using again a random generator and the assumed $\log N_H$ distribution. We computed unobscured 2-10 keV luminosities from infrared luminosities, and then X-ray fluxes by folding a power law spectrum with spectral energy index of 0.8 reduced at low energy by photoelectric absorption with a Chandra response matrix, computed by averaging the response at the off-axis positions of the real $24\mu\text{m}$ sources. For column densities $\gtrsim 10^{25} \text{cm}^{-2}$ we assumed that the direct emission is completely blocked by photoelectric absorption and Compton scattering. For these sources we assumed a reflection component with normalization 1/100 of the direct component and same spectral index. A small fraction of the simulated count rates (20-30%) is higher than the Chandra detection limit. These count rates have been excluded from the following anal-

ysis. The result of the simulations is shown in figure 4, right panel. According to our simulations, the average hardness ratio of the $\text{MIR}/\text{O} > 1000$ and $\text{R-K} > 4.5$ source sample without X-ray detection is reproduced if $80 \pm 10\%$ of the sources in the sample are highly obscured AGNs. The hardness ratio of the sources with $\text{MIR}/\text{O} < 200$ and $\text{R-K} > 4.5$ is reproduced if the fraction of the obscured AGN is smaller than 40%. Changing the assumptions made to produce the simulations within reasonable ranges changes only slightly this result. To account for these systematic uncertainties we increase by an additional 5% the confidence intervals of the AGN fraction. The result of the simulations is broadly consistent with the indication coming from the 1-24 μm SED fitting with galaxy and AGN templates. The observed SEDs of $\text{MIR}/\text{O} < 200$ and $\text{R-K} > 4.5$ sources are best fitted by AGN templates in $\sim 36\%$ of the cases, about half of the fraction of best fit AGN templates for the $\text{MIR}/\text{O} > 1000$ and $\text{R-K} > 4.5$ source sample.

4. DISCUSSION AND CONCLUSIONS

We selected a source sample with extreme mid-infrared to optical flux ratio ($\text{MIR}/\text{O} > 1000$) and red optical colors ($\text{R-K} > 4.5$) in the GOODS CDFS area. These sources are among the most luminous sources in the GOODS 24 μm sample, because of the correlation of MIR/O with the infrared luminosity (see figures 1 and 3 right panel). The fraction of these sources not directly detected in the Chandra images produces a significant stacked signal in both Chandra soft and hard X-rays bands. A detailed analysis based on Montecarlo simulation shows that the stacked count rates and hardness ratios can be reproduced if this source population is dominated by highly obscured ($N_{\text{H}} > \text{a few} \times 10^{23} \text{ cm}^{-2}$) AGNs. This conclusion is further confirmed by the following consideration. If we assume that this source population is dominated by star-forming galaxies, we can use the observed infrared luminosity and the dust-corrected UV luminosities to derive two star-formation rates. The median logarithmic star-formation rate from infrared luminosity is $2.31 (0.59) M_{\odot}/\text{yr}$. The median logarithmic UV star-formation rate is $0.83 (0.80) M_{\odot}/\text{yr}$, a factor 30 lower. The large mismatch between these two estimates strongly suggests that the infrared luminosity of this source sample is not dominated by star-formation but rather by accretion. As a comparison, the median infrared and UV star-formation rates of the sources with $\text{MIR}/\text{O} < 200$ and $\text{R-K} > 4.5$ in our control sample are 1.26 (0.38) and 1.10 (0.30), broadly consistent with each other, suggesting that the infrared luminosity of these sources is not dominated by accretion.

We can now compare the number of highly obscured AGNs selected at 24 μm and not detected in X-rays, with the number of unobscured and moderately obscured AGNs directly seen in the X-ray images. To limit the importance of complex selection effects we limit this analysis to the sources in the redshift bin 1.2-2.6. At $z=2.6$ the infrared luminosity corresponding to the limit of 40 μJy at 24 μm is of the order of $\log(\text{LIR})=44.8$. This suggests to limit the comparison to the sources with $\log\text{L}(2-10 \text{ keV}) > 43$ and $\log\text{L}(\text{IR}) > 44.8$. In the 1.2-2.6 redshift bin there are at least 38 sources with $\text{MIR}/\text{O} > 1000$, $\text{R-K} > 4.5$ and no direct X-ray detection, which are probably highly obscured AGNs (65% of 58 sources), and 44

X-ray selected AGNs, 7 of which with broad lines in their optical spectra. The number of 24 μm selected, presumably highly obscured AGNs, missed by the CDFS X-ray survey is therefore of the same order of magnitude of the number of X-ray selected AGNs.

The median infrared luminosity of the $\text{MIR}/\text{O} > 1000$ and $\text{R-K} > 4.5$ is 45.48 (0.59), implying a median intrinsic 2-10 keV luminosity of 43.68, adopting our assumption on the infrared to X-ray flux ratio. At $z=1.2$ and 2.6 this luminosity translates to X-ray fluxes between 10^{-14} and $10^{-15} \text{ erg cm}^{-2} \text{ s}^{-1}$, meaning that these sources would have been easily detected if they were not highly obscured.

In order to determine whether the highly obscured AGNs detected by the stacking technique are truly Compton thick we have compared our findings with the predictions of the La Franca et al. (2005) and Gilli et al. (2007) models. In the redshift bin 1.2-2.6 and in the area covered by our 24 μm sample the La Franca et al. (2005) luminosity function predicts about 75 AGNs with $\log\text{L}(2-10 \text{ keV}) > 43$ or $\log\text{L}(\text{IR}) > 44.8$, 20 of which with a column density $\gtrsim 10^{24} \text{ cm}^{-2}$. The absorption distribution adopted by the Gilli et al. (2007) AGN synthesis model for the Cosmic X-ray Background predicts about 40 Compton Thick AGNs with the same limits for redshift and luminosity. We find at least 38 24 μm selected, highly obscured AGNs a number similar to the Gilli et al. (2007) prediction and about twice the La Franca et al. (2005) prediction. In conclusion, according to the former model the population of infrared selected, highly obscured AGNs should be dominated by Compton thick objects, while according to the latter model roughly half of the sample should be made by Compton thick objects. In any case, the population of infrared selected, highly obscured AGNs is of the right size to reconcile the predictions of models of galaxy evolution with the observed moderate luminosity AGN number densities at $z > 1.2$ (e.g. Menci et al. 2004). It also helps in reducing substantially the discrepancy between the “active” SMBH mass function with the “relic” SMBH mass function (Marconi et al. 2004).

Our analysis is limited to AGNs of intermediate to high luminosity. Many more lower luminosity, highly obscured AGNs are certainly present in the infrared selected samples. The identifications of these sources, and therefore the extension of these results to lower AGN luminosities, requires a much more complex analysis. The observations that will be performed in a few years by the Herschel telescope at longer wavelengths (from 75 to 500 μm) will greatly help to this purpose.

Most of the GOOD-MUSIC 24 μm selected sources with high MIR/O , high R-K and no X-ray detection have a very faint optical and near infrared counterpart, only 14% of the sample having $\text{R} \lesssim 26$. Furthermore, only a handful of objects have a mid infrared flux high enough ($F(24\mu\text{m}) \gtrsim 0.5 \text{ mJy}$) to allow Spitzer IRS spectroscopy. The spectroscopic identification of $\sim 90\%$ of the sample must therefore await the advent of ELTs or the launch of JWST.

We are grateful to Fabio La Franca and Roberto Maiolino for useful discussions. Part of this work was supported by ASI/INAF contract I/023/05/0. Part of

this work was supported by the Deutsches Zentrum für Luft- und Raumfahrt, DLR project numbers 50 OR 0207 and 50 OR 0405.

REFERENCES

- Alexander, D. M., Bauer, F. E., Brandt, W. N. et al. 2003, *AJ*, 126, 539
- Alonso-Herrero, A. et al. 2006, *ApJ*, 640, 167
- Barmby, P., Alonso-Herrero, A., Donley, J.L. et al. 2006, *ApJ*, 642, 126
- Bongiorno, A. et al. 2007, *A&A* submitted, astro-ph/0704.1660
- Brandt, W.N., Hasinger, G. 2005, *ARA&A*, 43, 1056
- Brusa, M., Comastri, A., Daddi, E. et al. 2005 *A&A*, 432, 69
- Cavaliere, A. & Vittorini, V 2000, *ApJ*, 543, 599
- Cocchia, F., Fiore, F., Vignali, C. et al. 2006, *A&A*, 466, 31
- Comastri, A. 2004, in "Supermassive Black Holes in the Distant Universe", Ed. A. J. Barger, Kluwer Academic, vol. 308, p.245
- Cowie L.L., Songaila, A., Hu, E.M., Cohen, J.G., 1996, *AJ*, 112, 839
- De Lucia, G., Springel, V., White, S.D.M., Croton, D., Kauffmann, G., 2006, *MNRAS*, 366, 499
- De Santis, C., Grazian, A., Fontana, A., Santini, P. 2007, *New Astronomy*, 12, 271
- Di Matteo, T., Springel, V., Hernquist, L. 2005, *Nature*, 433, 604
- Eckart, M.E., Stern, D., Helfand, D. et al. 2006, *ApJS*, 165, 19
- Fabian, A.C. 1999 *MNRAS*, 308, L39
- Ferrarese, L. & Merrit, D. 2000, *ApJ*, 539, L9
- Fiore, F., Brusa, M., Cocchia, F. et al. 2003, *A&A*, 409, 79
- Franceschini, A., Hasinger, G., Miyaji, T., Malguori, D. 1999, *MNRAS*, 310, L5
- Gebhardt, K., Kormendy, J., Ho, L. et al. 2000, *ApJ*, 543, L5
- Giacconi, R., Zirm, A., Wang, J., et al. 2002, *ApJS*, 139, 369
- Gilli R., Salvati, M., Hasinger G. 2001, *A&A*, 366, 407
- Gilli R., Comastri A., Hasinger G. 2007, *A&A*, 463, 79
- Hasinger, G. 2003, *AIP Conf. Proc.* 666, 227
- Hasinger, G., Miyaji, T., Schmidt, M. 2005 *A&A*, 441, 417
- Houck, J.R., et al. 2005, *ApJ*, 622, L105
- Lacy, M. et al. 2004, *ApJS*, 154, 166
- La Franca, F., Fiore, F., Comastri A. et al. 2005, *ApJ*, 635, 864
- Granato, G.L., Silva, L., Monaco, P., Panuzzo, P., Salucci, P., De Zotti, G., & Danese, L. 2001, *MNRAS*, 324, 757
- Granato, G.L., De Zotti, G., Silva, L., Bressan, A., Danese, L. 2004, *ApJ*, 600, 580
- Grazian, A., Fontana, A., de Santis, C. et al. 2006, *A&A*, 449, 951
- Marconi, A., Hunt, L. 2003, *ApJ*, 589, L21
- Marconi, A., Risaliti, G., Gilli, R., Hunt, L. K., Maiolino, R., Salvati, M. 2004, *MNRAS*, 351, 169
- Matt. G. 2000, *A&A*, 355, L31
- Martinez-Sansigre, A., Rawlings, S., Lacy, M. et al. 2005, *Nature*, 436, 666
- Menci N., Fiore, F., Perola, G.C, Cavaliere, A. 2004, *ApJ*, 606, 58
- Menci, N., Fontana, A., Giallongo, E., Salimbeni, S. 2005 *ApJ*, 632, 49
- Polletta, M., Wilkes, B., Siana, B. et al. 2006, *ApJ*, 642, 673
- Polletta, M., Tajer, M., Maraschi, L. et al. 2007, *ApJ* in press, astro-ph/0703255
- Pozzi, F., Vignali, C., Comastri, A. et al. 2007, *A&A* in press, astro-ph/0704.0735
- Ranalli, P., Comastri, A., Setti, G. 2003, *A&A*, 399, 99
- Sanders, D.B., Mirabel, I.F. 1996, *ARA&A*, 34, 749
- Silk, J., Rees, M.J. 1998, *A&A*311, L1
- Soltan, A. 1982, *MNRAS*, 200, 115
- Tozzi, P. , Gilli R. Mainieri V. et al. 2006, *A&A*, 451, 457
- Ueda Y., Akiyama M., Ohta K., Miyaji T. 2003, *ApJ*, 598, 886
- Weedman, D.W., Le Floch, E., Higdon, S.J.U., Higdon, J.L., Houck, J.R. 2006a *ApJ*, 638, 613
- Weedman, D.W., Soifer, B.T., Hao, L. et al. 2006b, *ApJ*, 651, 101
- Worsley, M.A., Fabian, A. C., Barcons, X. et al. 2004, *MNRAS*, 352, L28
- Worsley, M.A., Fabian, A. C., Bauer, F.E., Alexander, D.M., Brandt, W.N., Lehmer, B.D. 2006, *MNRAS*, 368, 1735